Effects of Fe$_2$O$_3$ addition on the electrical properties of SDC solid electrolyte ceramics

Jihai Cheng[1] · Changan Tian[1] · Jie Yang[1]

Abstract

Ceria-based electrolyte powders consisting of Fe$_2$O$_3$ and Sm$_2$O$_3$ double-doped ceria (Ce$_{0.8}$Sm$_{0.2-x}$Fe$_x$O$_{2-\delta}$) were synthesized by a sol–gel method. The structure and electrochemical characters of the electrolyte materials have been studied. The phase formation of precursor powders was studied by the X-ray diffraction analysis (XRD). Microstructural and sinterability measurements were carried out on the sintered electrolyte discs. Electrochemical impedance spectroscopy (EIS) was used for estimate the electrochemical properties. The results displayed that crystalline cubic fluorite structured is formed after calcined at 700 °C. The electrochemical analysis results showed that the electrical properties of Ce$_{0.8}$Sm$_{0.2}$O$_{1.9}$ (SDC) electrolytes substituted with certain Fe$_2$O$_3$ were superior and a total conductivity of 0.0263 S cm^{-1} could be obtained in the $x = 0.1$ sample. Therefore, it was concluded that co-doped with Fe$_2$O$_3$ and Sm$_2$O$_3$ could enhance the electrical conductivities of CeO$_2$-based solid electrolyte, indicating that it is a potential electrolyte for SOFCs.

1 Introduction

With the development of the society, energy affects all sectors of the global economy. The increasing industrialization requires sustainable, highly efficient energy production. Solid oxide fuel cell (SOFC) is a type of electrochemical device that can convert chemical energy into electric energy efficiently and environment-friendly [1–3]. In SOFC, several doped ceria materials were identified as attractive electrolytes because of the high ionic conductivity [4–11]. The substitution of trivalent ions for Ce^{4+} ions can enhance the vacancies number and result in the increasing of oxygen ion conductivities in ceria-based materials, so rare earth ions doped ceria exhibit high conductivity [12–16]. When CeO$_2$-based electrolyte doped with a trivalent rare earth metal oxide or a divalent alkaline earth metal oxide, the oxygen vacancies formed in the oxygen sublattice due to the charge compensation, thereby increasing the ionic conductivity. The total conductivity (σ_{tot}) of a polycrystalline CeO$_2$-based electrolyte is determined by the grain conductivity (σ_{gi}) and the grain boundary conductivity (σ_{gb}). σ_{gi} is usually 100–1000 times higher than σ_{gb} [17, 18]. During the

sintering process, there are a certain amount of impurities exist at grain boundaries which increase the grain boundary resistance and resulting in the decrease of σ_{gb}.

In the study of ceria-based materials, double doped ceria is found to have superior electrical properties. Ceria-based electrolytes co-doped with alkaline earth (Ca^{2+}, Sr^{2+}) and rare earth ions (Gd^{3+}, Sm^{3+}, Y^{3+}) have been extensively studied in the past decade years. In addition, to further improve the ionic conductivity, co-doped samples such as Ce$_{0.8}$Ln$_{0.2-x}$M$_x$O1.9 (Ln = La, Gd, Sm, M = Y, Mg, Pr, etc.) have been studied [19, 20]. Usually, ceria-based materials co-doped with alkaline earth and rare earth ions were sintered at high temperature in order to obtain dense solid electrolyte with a single-phase of cubic fluorite structure for SOFC applications. In order to improve the densification, the sintering aids such as CuO and MnO$_2$ have been added [21]. Duncan P. Fagg reported small (2 mol%) cobalt oxide additions to ceria-gadolinia materials considerably improve sinterability, making it possible to obtain ceramics with 95–99% density [22].

CeO$_2$-based electrolytes doping with transition metal oxides such as Co$_2$O$_3$, Fe$_2$O$_3$ and Al$_2$O$_3$ have a certain effect on scavenging impurities in the electrolyte materials, which can improve the grain boundary conductivity and total conductivity [23–25]. Among them, Fe$_2$O$_3$ can be used not only as a impurities degreaser at grain boundaries, but also has the role of sintering aids for CeO$_2$-based electrolyte [26, 27].

✉ Jihai Cheng
jhcheng256@163.com

1 Department of Chemistry and Materials Engineering, Hefei University, Hefei 230601, China

Ceria-based materials are often prepared by conventional solid-state reactions, lower temperature reactions including hydrothermal, precipitation, auto-combustion and other soft chemical processes [28–31]. Among these, the sol–gel method offers a new way to prepare electrolyte powders because of its advantages such as short reaction time, and it is simple more efficient than other methods. Moreover, high purity products with small particle sizes and narrow particle size distributions can be obtained from the sol–gel process [32].

In this study, Fe_2O_3 and Sm_2O_3 double-doped ceria-based electrolyte powders have been prepared by sol–gel process. The samples were characterized using thermogravimetric and differential scanning calorimetry (TG–DSC), X-ray diffraction (XRD), scanning electron microscope (SEM) and electrochemical impedance spectroscopy (EIS). The results of this work can contribute to the fabrication of novel electrolyte for the application to SOFC devices.

2 Experimental

2.1 Sample preparation

$Ce_{0.8}Sm_{0.2-x}Fe_xO_{2-\delta}$ ($x = 0$–0.2) ultrafine powders were prepared by the sol–gel method. In the process, analytical pure cerium nitrate ($Ce(NO_3)_3 \cdot 6H_2O$), samarium nitrate ($Sm(NO_3)_3 \cdot 6H_2O$) and $Fe(NO_3)_3 \cdot 9H_2O$ were used as the raw materials.

During the preparation process, the aforementioned three nitrates were dissolved in deionized water and mixed together, citric acid was then added as complexing agents to form a homogenous solution, the molar ratio of citric acid to metal ion (Ce, Sm, Fe) is 1.5:1. The above mixture was continuously stirred using a magnetic agitator to form a homogenous solution at 80 °C, then converted to a viscous gel. The gel was dried in an oven at 120 °C for 24 h

to remove the solvents, and then calcined at 700 °C for 2 h in a muffle furnace. The synthesized $Ce_{0.8}Sm_{0.2-x}Fe_xO_{2-\delta}$ powders were pressed into discs with size of $\phi 11 \times 1$ mm, finally sintered at 1400 °C for 4 h in air atmosphere to obtain wafers used for testing purposes.

2.2 Materials characterisation

$Ce_{0.8}Sm_{0.2-x}Fe_xO_{2-\delta}$ xerogels were studied using TG–DSC simultaneous thermal analyzer (Netzsch STA 409PC, Germany) in a nitrogen atmosphere. The phase composition of the calcined $Ce_{0.8}Sm_{0.2-x}Fe_xO_{2-\delta}$ powders was analyzed by X-ray diffraction (XRD) method (Rigaku, Japan), the diffractograms were scanned in 2θ from 20° to 70° using Cu Kα line ($\lambda = 0.154056$ nm). The microstructure was analyzed with a scanning electron microscope (SEM, Model S4800). The electrochemical performance of the sintered discs was tested using an electrochemical analyzer (CHI660D, China). For electrochemical testing, silver paste was coated uniformly on both sides of each sintered disc and then fired at 700 °C for 10 min to form Ag electrodes. Measurement of the data were conducted in the frequency range 0.1 Hz–100 kHz from 400 to 800 °C in increments of 50 °C, the obtained impedance spectra were processed using ZSimpWin software.

3 Results and discussion

3.1 TG–DSC analysis

The thermal evolution of the xerogels were analyzed by recording TG–DSC curves. As shown in Fig. 1, the thermal decomposition and weightlessness of the xerogels can be divided into three stages. The first stage: from room temperature to 160 °C, the weight loss of the sample is about 7.6%, which corresponds to the loss of adsorbed water and citric acid in

Fig. 1 TG–DSC curves of $Ce_{0.8}Sm_{0.2-x}Fe_xO_{2-\delta}$ ($x = 0.1$) xerogel
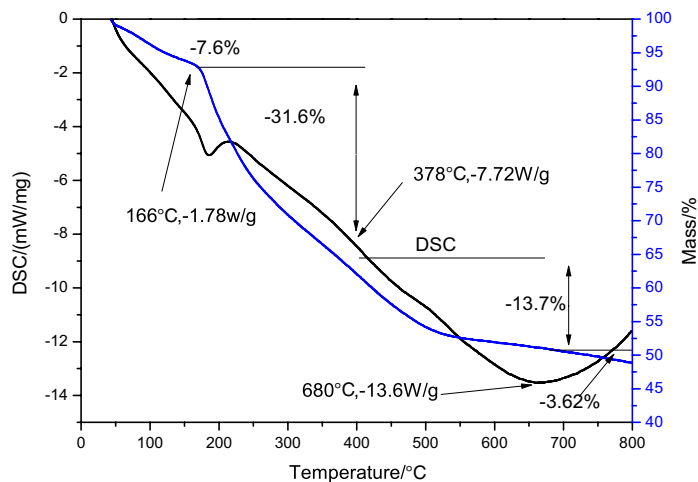
the sample. In the second stage(160–650 °C), there is a strong exothermic peak on the DSC curve and the weight loss of the sample is about 45%, corresponding to the decomposition process of some organic groups and ions in the sample. When the temperature is above 650 °C, the change of TG curve is not obvious, which indicates that the decomposition of organic matter in the sample has been completed. However, an obvious exothermic peak appears in the DSC curve at about 670 °C, which may be formed by the phase transition and crystallization process of the sample, indicating that a solid solution of $Ce_{0.8}Sm_{0.2-x}Fe_xO_{2-\delta}$ has been formed at this temperature. By analyzing the thermal behavior of $Ce_{0.8}Sm_{0.2-x}Fe_xO_{2-\delta}$ xerogels, precursor powders were calcined at 700 °C for 2 h in present study.

3.2 XRD analysis

Figure 2 shows the XRD patterns of the $Ce_{0.8}Sm_{0.2-x}Fe_xO_{2-\delta}$ powders along with CeO_2 standard patterns with cubic fluorite structure. $Ce_{0.8}Sm_{0.2-x}Fe_xO_{2-\delta}$ powders calcined at 700 °C crystallized well, and no second phase can be recognized. The powders showing all main reflections corresponding to the reference spectra (JCPDS No. 43-1002), indicative of the complete formation of CeO_2-based solid solution with typical cubic fluorite structure.

The crystallite sizes were calculated using the Scherrer equation [33]:

$$D = 0.9\lambda/\beta\cos\theta \tag{1}$$

where D is the crystallite size, λ is the X-ray radiation wavelength, 2θ represents the diffraction angle and β is the strongest Bragg's peak corresponding to the reflection for the samples. $\beta = \sqrt{\beta_m^2 - \beta_s^2}$ is the corrected FWHM of the
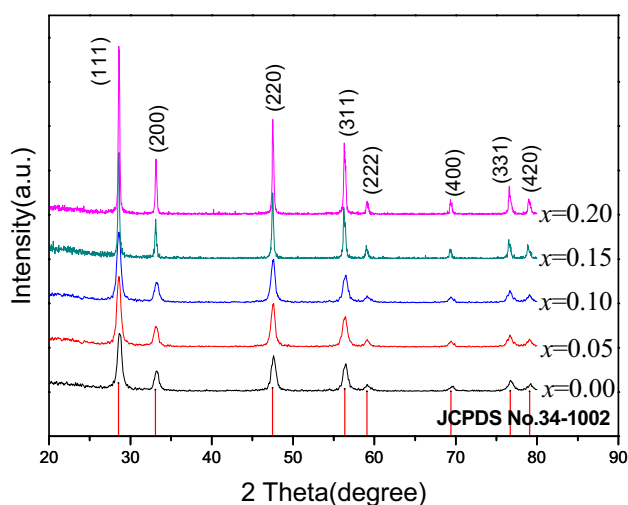
observed halfwidth: β_m is that of the (111) reflection in samples and β_s is that of the (111) reflection in a standard sample (Si from NIST). Table 1 shows the cell parameters of the samples calculated from the XRD patterns using Jade software.

Fe^{3+} co-doping decreases the lattice constant compared to SDC as expected from effective ionic radii considerations [34]. The SDC powder lattice parameter ($a = 0.5433$ nm) is slightly bigger than that of pure ceria ($a = 0.5411$ nm, in accordance with JCPDS card 43-1002), while co-doping with Fe^{3+} leads to a decrease in the lattice parameter, which attribute to the ionic radius of Fe^{3+} (0.065 nm) is smaller than that of Sm^{3+} (0.108 nm) and Ce^{4+} (0.097 nm). The lattice parameters depend on the ionic radius, amount, and solubility limit of the dopant ions, thus the lattice parameter of SDC decreases as the Fe content increasing [35–37].

3.3 Microstructure and sinterability analysis

Figure 3a–c display the SEM micrographs of the discs sintered at 1400 °C. The image show that the discs were dense and uniform. There are no obvious cracks and pores at the interface of the samples. It indicates good sintering of $Ce_{0.8}Sm_{0.2-x}Fe_xO_{2-\delta}$ samples. The mean grain sizes of the pellet was approximately 1–5 μm.

In order to estimate the influence of sintering temperature to the density of electrolyte ceramics, the $Ce_{0.8}Sm_{0.2-x}Fe_xO_{2-\delta}$ samples were sintered at different temperatures. Figure 3d–f display the surface topography of $Ce_{0.8}Sm_{0.1}Fe_{0.1}O_{2-\delta}$ sintered at 1100 °C, 1200 °C and 1300 °C, respectively. It can be found that the density of the sample increased with the increasing of sintering temperature. There are many pores on the surface of sintered sample at low temperatures (1100 °C and 1200 °C, Fig. 3d, e), while the pores on the surface of the sample are less and less with the increase of sintering temperature. There are no obvious pores at the interface of the samples which sintered at 1400 °C (Fig. 3b).Based above discussions, the samples should sintered at 1400 °C to form dense electrolyte ceramics.

Fig. 2 XRD patterns of the $Ce_{0.8}Sm_{0.2-x}Fe_xO_{2-\delta}$ powders (red vertical lines represent the standard diffraction peak of the CeO_2) (Color figure online)

Table 1 Measured and calculated properties of the $Ce_{0.8}Sm_{0.2-x}Fe_xO_{2-\delta}$ samples

x	Lattice parameter a (nm)	D_{XRD} (nm)	ρ_{th} (g cm^3)	Relative densities (%)
0	0.5433	15.4	6.85	98.74
0.05	0.5424	14.6	6.79	98.30
0.10	0.5412	13.3	6.74	97.68
0.15	0.5409	13.9	6.68	95.41
0.20	0.5398	12.1	6.62	99.27

Fig. 3 SEM micrographs of the $Ce_{0.8}Sm_{0.2-x}Fe_xO_{2-\delta}$ sintered discs (different dopant content x sintered at 1400 °C: **a** 0.05; **b** 0.1; **c** 0 and 1% mol content sintered at: **d** 1100 °C, **e** 1200 °C, **f** 1300 °C)
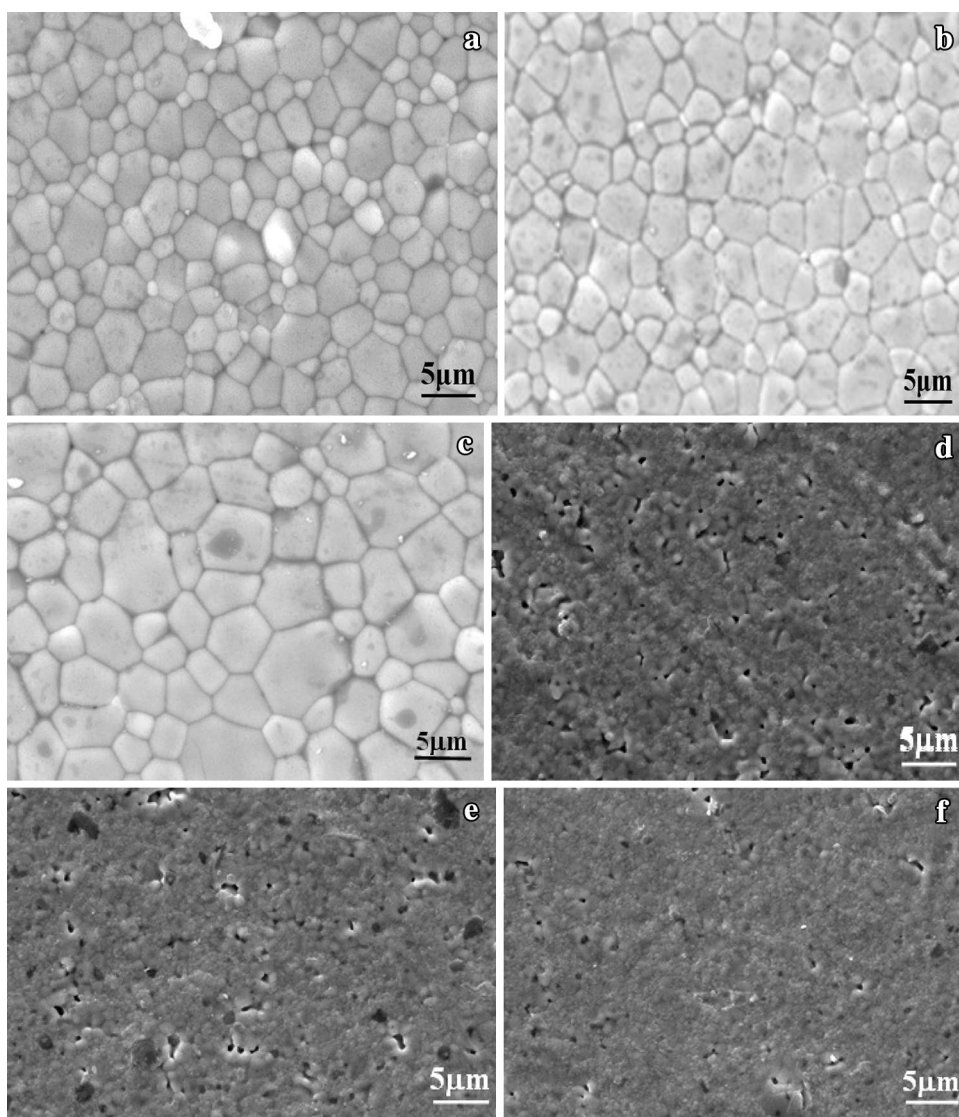
The bulk density (ρ) and open porosity of $Ce_{0.8}Sm_{0.2-x}Fe_xO_{2-\delta}$ sintered discs was measured using Archimedes method with deionized water:

$$\rho = \frac{W_{Dry} \times \rho_{Water}}{W_{Wet} - W_{Sus}} \qquad (2)$$

where W_{Dry} is the weight of sintered discs, ρ_{water} is the density of water (0.997 g·cm^{-3}), W_{Wet} is the wet weight (boil the discs in water for 30 min), and W_{sus} represents the suspended weight of sintered discs in water. The relative density of $Ce_{0.8}Sm_{0.2-x}Fe_xO_{2-\delta}$ discs sintering at 1400 °C reached above 95%, which confirmed that the sintered discs were dense with low porosity. The results of density and porosity testing showed that $Ce_{0.8}Sm_{0.2-x}Fe_xO_{2-\delta}$ powders prepared by sol–gel method have good sinterability.

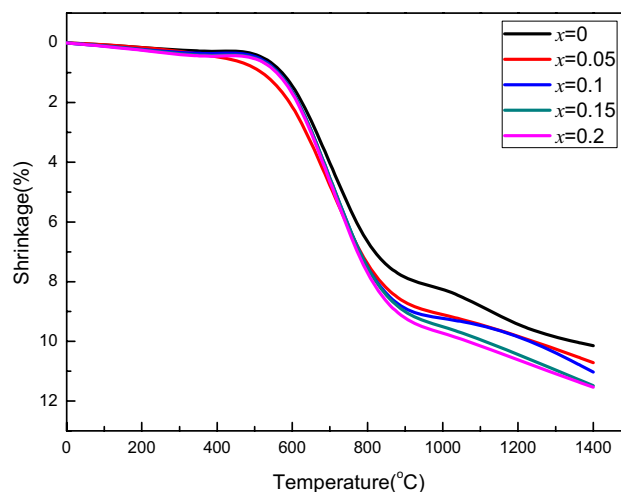Figure 4 illustrates the shrinkage curves of the $Ce_{0.8}Sm_{0.2-x}Fe_xO_{2-\delta}$ samples. The onset of $Ce_{0.8}Sm_{0.2-x}Fe_xO_{2-\delta}$

Fig. 4 Shrinkage curves of $Ce_{0.8}Sm_{0.2-x}Fe_xO_{2-\delta}$ samples as a function of sintering temperature

shrinkage occurred at lower temperature and rapid shrinkage occurred over a narrow temperature region (600–900 °C), and final shrinkage was approximately 12%. When the temperature is above 1400 °C, the change of shrinkage curve is not obvious, which indicates that the density of the samples were high. Thus, we selected 1400 °C as the sintering temperature, as it is sufficient to obtain the dense electrolyte ceramics.

3.4 Electrochemical analysis

Electrochemical impedance spectroscopy (EIS) is a powerful electrochemical technique with wide applications in SOFC development. It can characterize the information of ohmic losses, electrochemical kinetics, and mass transfer processes individually. It can obtain a symmetrical cell from a representative impedance spectrum, R_b and R_{gb} are the bulk and grain-boundary resistances of the electrolyte, R_e is the electrode resistance. There are two semicircles of the electrolyte process in such circuit at high frequencies are represented by two resistances, R_b and R_{gb} [38].

The conductivities of Fe doped SDC electrolyte ceramics were measured in air atmosphere. Figure 5 shows the electrochemical impedance spectra of sintered discs ($x = 0.1$). As seen in Fig. 5, there are two incomplete semicircles in the spectrum at lower testing temperatures corresponded to grain boundary and electrode interface resistance, respectively [39]. As the increasing of operating temperature, the first arc reduced gradually, when working temperature reached 800 °C, there is only a single depressed arc can be observed in the impedance spectra. From the intercepts of the semicircular arcs at "z" axes, it can obtain the values of R_b and R_{gb} [29, 31, 40]. Based on the resistance values, using the following equation, it can calculate the conductivities of Fe doped SDC electrolytes.

$$\sigma = \frac{L}{R \times S} \tag{3}$$

where L is the thickness of sintered disc, R is total resistance, S represents the electrode area of the sample. Conductivities and activation energies of the samples tested at 800 °C are listed in Table 2.

From the conductivities calculated results, the conductivity of $Ce_{0.8}Sm_{0.2-x}Fe_xO_{2-\delta}$ ceramics increases with the increasing of Fe content and reaches a maximum at $x = 0.1$, then decreases. On one hand, the grain grows due to the doping of Fe_2O_3 (shown as Fig. 3), so the contact between the grains is tighter, the density is increased and reduced the grain resistance, thus increasing the grain conductivity. On the other hand, oxygen vacancies formed when SDC doped with the trivalent Fe^{3+} ion, and most of these oxygen vacancies are mobile in lower dopant content range, which result the increase in conductivity. But defect
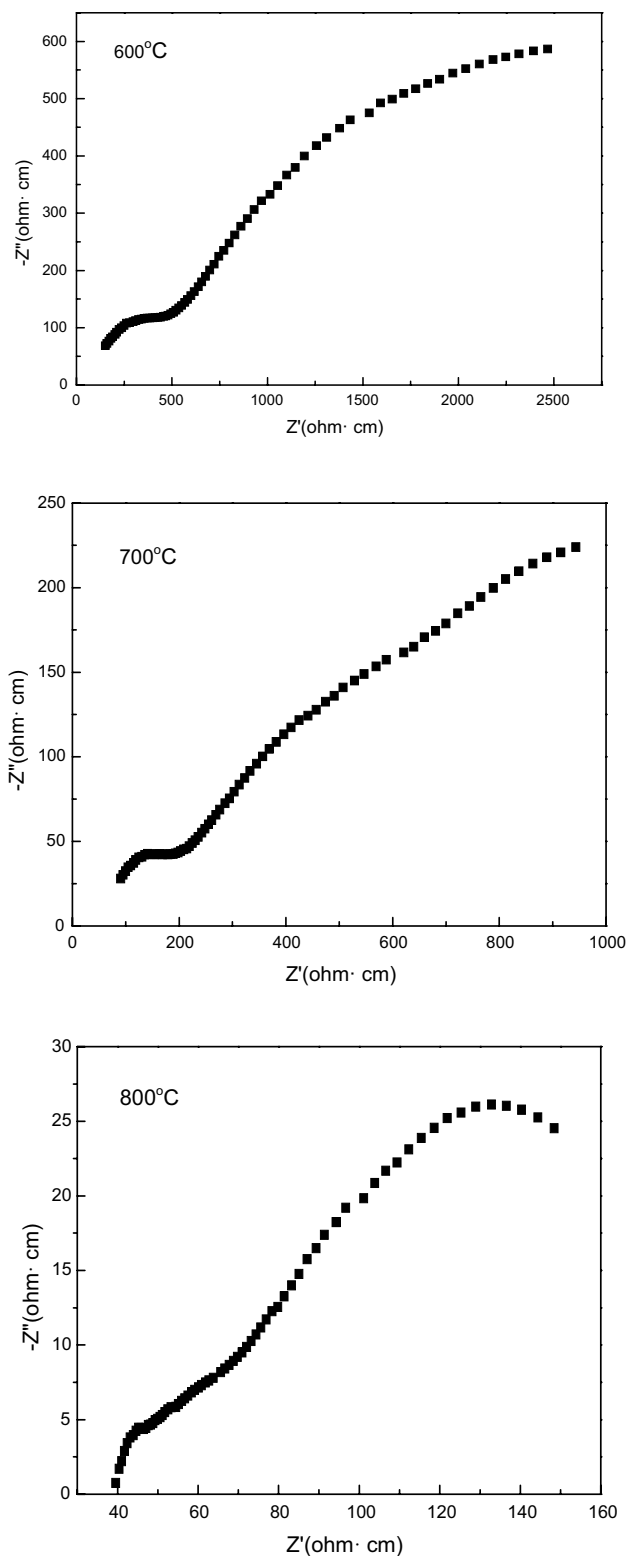

Fig. 5 Electrochemical impedance spectra of sintered discs ($x = 0.1$) operated at different temperatures

Table 2 Conductivities and activation energies of the samples tested at 800 °C

x	R_{total} (Ω)	σ (S cm^{-1})	Ea (eV)
0	9.7525	0.015	0.85
0.05	6.6495	0.022	0.82
0.10	4.3263	0.026	0.77
0.15	8.1271	0.018	0.90
0.20	12.1907	0.012	1.14

associations formed at the cost of oxygen vacancies as doped Fe content increasing, so the conductivity decreased [41, 42]. Furthermore, doping Fe_2O_3 in SDC, there will be a small amount of Fe^{3+} entering the lattice to replace Ce^{4+} to generate oxygen vacancies:

$$FeO_{1.5} \xrightarrow{CeO_2} Fe'_{Ce} + \frac{1}{2}V_O^{\cdot\cdot} + \frac{3}{2}O_O \tag{4}$$
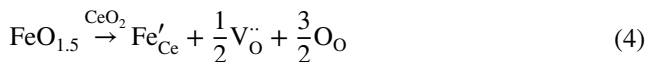
Because the attraction between Fe'_{Ce} and $V_O^{\cdot\cdot}$ is greater than that of Sm'_{Ce} and $V_O^{\cdot\cdot}$, so Fe'_{Ce} and $V_O^{\cdot\cdot}$ are easier to combine. When the doping amount of Fe_2O_3 is higher than $0.1(x)$, part of Fe^{3+} enters SDC lattice to replace Ce^{4+} to produce Fe'_{Ce}. Fe'_{Ce} combines with $V_O^{\cdot\cdot}$, to form an association defect $[Fe'_{Ce} \cdot V_O^{\cdot\cdot}]$ [43, 44]. It can be seen from formula (4), two Fe^{3+} ions will generate one oxygen vacancy, however, a Fe^{3+} ion will associate one free oxygen vacancy ($[Fe'_{Ce} \cdot V_O^{\cdot\cdot}]$), which reduces the concentration of oxygen vacancies, and decreases the conductivity. All in all, doping Fe_2O_3 may have two effects on the SDC system: one is that Fe_2O_3 scavenges the impurities exist at grain boundaries to increase the conductivity; the second is that Fe'_{Ce} and $V_O^{\cdot\cdot}$ combine to form the association $[Fe'_{Ce} \cdot V_O^{\cdot\cdot}]$, which results the decreasing of oxygen vacancies concentration and conductivities. The effects of the above two aspects resulted in the fact that SDC shows the superior conductivity with certain Fe_2O_3 content ($x=0.1$). The electrical behavior of $Ce_{0.8}Sm_{0.2-x}Fe_xO_{2-\delta}$ ceramics was similar to other rare earth ions doped ceria electrolytes [45–48]. It demonstrates that the electrical properties of the ceria-based electrolyte could be enhanced doped with appropriate Fe content in SDC could enhance for SOFCs applications.

Representative Arrhenius plots of the reciprocal temperature dependence of log(σT) of $Ce_{0.8}Sm_{0.2-x}Fe_xO_{2-\delta}$ electrolytes are shown in Fig. 6 which follows the Arrhenius equation:

$$\sigma = \frac{A}{T} \exp\left(-\frac{E_a}{KT}\right) \tag{5}$$

The activation energies calculated from Fig. 5 reach a minimum at $x=0.1(0.77 \text{ eV})$.
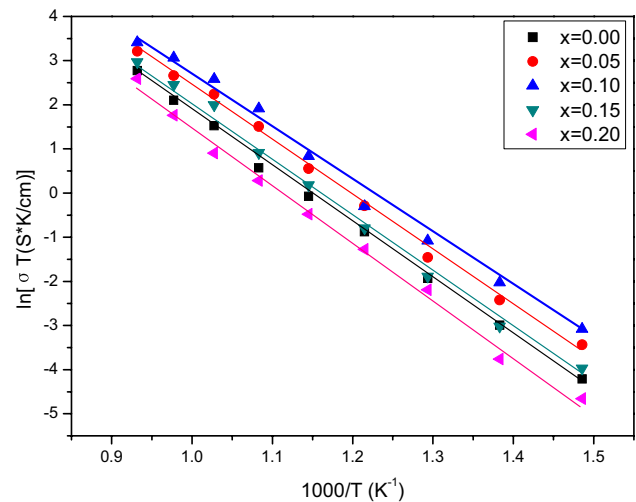
Fig. 6 Arrhenius plots of the conductivities of $Ce_{0.8}Sm_{0.2-x}Fe_xO_{2-\delta}$ solid electrolyte

In the study of electrochemical properties of ceria-based materials, the interaction between dopant M'_{Ce} or M''_{Ce} and oxygen vacancies $V_O^{\cdot\cdot}$, resulting the formation of associates $2M'_{Ce} - V_O^{\cdot\cdot}$ or $M''_{Ce} - V_O^{\cdot\cdot}$. It needs an additional energy to free the vacancy from the association, so Arrhenius plot of conductivity often shows a kink towards low-temperature regime to reflect the increasing activation energy. Moreover, there is a minimization of the lattice elastic strain, so the maximum conductivity can be observed for a specific dopant with the closest match in ionic radius of the dopant cation and Ce^{4+} in ceria based electrolytes. In reducing atmospheres, the excess electronic conduction can considerably elevates due to the presence of a variable Ce valence which named Ce^{3+} (Ce'_{Ce}) and Ce^{4+} ($Ce^{\times}_{Ce}$) by the following defect reaction.

$$O_O^{\times} + 2Ce_{Ce}^{\times} = \frac{1}{2}O_2 + V_O^{\cdot\cdot} + 2Ce'_{Ce} \tag{6}$$
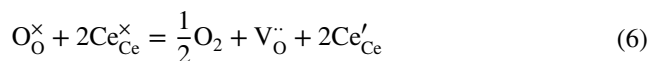
Based on the electrochemical measurements, we suggested that Sm and Fe co-doped CeO_2 composite material is a prospective electrolyte because of its superior electrochemical properties for future use in IT-SOFCs, and $Ce_{0.8}Sm_{0.2-x}Fe_xO_{2-\delta}$ directs a new strategy to design novel electrolyte materials for SOFCs applications.

4 Conclusion

$Ce_{0.8}Sm_{0.2-x}Fe_xO_{2-\delta}$ solid electrolyte powders were prepared by the sol–gel method. XRD studies confirmed the formation of ceria based electrolytes with cubic fluorite structure after doped with Sm^{3+} and Fe^{3+} ions. Microstructure measurements displayed that the $Ce_{0.8}Sm_{0.2-x}Fe_xO_{2-\delta}$ electrolyte

ceramics are quite dense and uniform with good sinterability after sintered at 1400 °C for 4 h, and the relative densities reached above 95%. Electrochemical analysis indicated the electrical conductivities of $Ce_{0.8}Sm_{0.2-x}Fe_xO_{2-\delta}$ electrolytes were much higher than that of SDC, and the dopant content at $x = 0.1$, the electrolyte showed the best ionic conductivity of 0.0263 S cm^{-1} at 800 °C. In summary, CeO_2-based solid electrolyte ceramics which doped with Fe and Sm had a potential application for solid oxide fuel cells in middle or low level temperatures range.

References

1. S. Prakash, B. Parthasarathi, S. Kumar, S.T. Aruna, Microstructure and electrical properties of plasma sprayed Gd 0.15 Ce 0.85 O 2 − δ coatings from solution combustion synthesized flowable powders. J. Eur. Ceram. Soc. **37**, 271–279 (2017)

2. C. Yao, J. Meng, X. Liu, X. Zhang, X. Liu, F. Meng, X. Wu, J. Meng, Enhanced ionic conductivity in Gd-doped ceria and (Li/Na)2SO4 composite electrolytes for solid oxide fuel cells. Solid State Sci. **49**, 90–96 (2015)

3. K.C. Anjaneya, G.P. Nayaka, J. Manjanna, V.M. Ashwin Kumar, G. Govindaraj, K.N. Ganesha, Investigation on the Sr-doped ceria Ce1 − xSrxO2 − δ (x = 0.05–0.2) as an electrolyte for intermediate temperature SOFC. J. Alloys Compd. **598**, 33–40 (2014)

4. A. Maheshwari, H.-D. Wiemhöfer, Sr₂₊–Gd₃₊ co-doped CeO₂: a cost-effective variant for IT-SOFC electrolytes. Ceram. Int. **41**, 9122–9130 (2015)

5. M. Dudek, M. Mosiałek, Utility of Ce0.8M0.2O1.9, Ce0.8M0.15Y0.05O1.9, M = Gd, Sm powders synthesized by aerosol decomposition method in solid oxide fuel cell technology. Electrochim. Acta **104**, 339–347 (2013)

6. T. Somekawa, Y. Matsuzaki, Y. Tachikawa, S. Taniguchi, K. Sasaki, Study of the solid-state reaction at the interface between lanthanoid-doped ceria and yttria-stabilized zirconia for solid-oxide fuel cell applications. Solid State Ion. **282**, 1–6 (2015)

7. N.C. Martins, S. Rajesh, F.M. Marques, Synthesis and electrochemical assessment of Ce0.5Yb0.5O1.75 ceramics and derived composite electrolytes. Mater. Res. Bull. **70**, 449–455 (2015)

8. L. Spiridigliozzi, M. Biesuz, G. Dell'Agli, E. Di Bartolomeo, F. Zurlo, V.M. Sglavo, Microstructural and electrical investigation of flash-sintered Gd/Sm-doped ceria. J. Mater. Sci. **52**, 7479–7488 (2017)

9. C. Rockenhäuser, B. Butz, N. Schichtel, J. Janek, R. Oberacker, M.J. Hoffmann, D. Gerthsen, Microstructure evolution and cation interdiffusion in thin Gd₂O₃ films on CeO₂ substrates. J. Eur. Ceram. Soc. **34**, 1235–1242 (2014)

10. H. Liu, J. Huang, D. Zhao, H. Yang, T. Zhang, Improving the electrical property of CeO₂-containing sealing glass–ceramics for solid oxide fuel cell applications: effect of HfO₂. J. Eur. Ceram. Soc. **36**, 917–923 (2016)

11. E.O. Oh, C.M. Whang, Y.R. Lee, S.Y. Park, D.H. Prasad, K.J. Yoon, J.W. Son, J.H. Lee, H.W. Lee, Extremely thin bilayer electrolyte for solid oxide fuel cells (SOFCs) fabricated by chemical solution deposition (CSD). Adv. Mater. **24**, 3373–3377 (2012)

12. S. Dutta, A. Nandy, A. Dutta, S.K. Pradhan, Structure and microstructure dependent ionic conductivity in 10 mol% Dy₂O₃ doped CeO₂ nanoparticles synthesized by mechanical alloying. Mater. Res. Bull. **73**, 446–451 (2016)

13. J.-E. Hong, S. Ida, T. Ishihara, Decreased sintering temperature of anode-supported solid oxide fuel cells with La-doped CeO₂ and Sr- and Mg-doped LaGaO₃ films by Co addition. J. Power Sources **259**, 282–288 (2014)

14. H. Tinwala, P. Shah, K. Siddhapara, D. Shah, J. Menghani, Investigation of ionic conductivity of lanthanum cerium oxide nano crystalline powder synthesized by co precipitation method. J. Cryst. Growth **452**, 54–56 (2016)

15. L. Guan, S. Le, X. Zhu, S. He, K. Sun, Densification and grain growth behavior study of trivalent MO1.5 (M = Gd, Bi) doped ceria systems. J. Eur. Ceram. Soc. **35**, 2815–2821 (2015)

16. K.C. Anjaneya, G.P. Nayaka, J. Manjanna, G. Govindaraj, K.N. Ganesha, Preparation and characterization of Ce1 − xGdxO2 − δ (x = 0.1–0.3) as solid electrolyte for intermediate temperature SOFC. J. Alloys Compd. **578**, 53–59 (2013)

17. B.C.H. Steele, Appraisal of Ce1 − yGdyO2 − y/2 electrolytes for IT-SOFC operation at 500°C. Solid State Ion. **129**, 95–110 (2000)

18. J.L.M. Rupp, A. Infortuna, L.J. Gauckler, Microstrain and self-limited grain growth in nanocrystalline ceria ceramics. Acta Mater. **54**, 1721–1730 (2006)

19. S.A. Muhammed Ali, M. Anwar, A.M. Abdalla, M.R. Somalu, A. Muchtar, Ce0.80Sm0.10Ba0.05Er0.05O2 − δ multi-doped ceria electrolyte for intermediate temperature solid oxide fuel cells. Ceram. Int. **43**, 1265–1271 (2017)

20. E.Y. Pikalova, A.A. Murashkina, V.I. Maragou, A.K. Demin, V.N. Strekalovsky, P.E. Tsiakaras, CeO₂ based materials doped with lanthanides for applications in intermediate temperature electrochemical devices. Int. J. Hydrog. Energy **36**, 6175–6183 (2011)

21. X. Zhang, C. Decès-Petit, S. Yick, M. Robertson, O. Kesler, R. Maric, D. Ghosh, A study on sintering aids for Sm0.2Ce0.8O1.9 electrolyte. J. Power Sources **162**, 480–485 (2006)

22. D.P. Fagg, V.V. Kharton, J.R. Frade, Transport in ceria electrolytes modified with sintering aids: effects on oxygen reduction kinetics. J. Solid State Electrochem. **8**, 618–625 (2004)

23. W. Zając, L. Suescun, K. Świerczek, J. Molenda, Structural and electrical properties of grain boundaries in Ce0.85Gd0.15O1.925 solid electrolyte modified by addition of transition metal ions. J. Power Sources **194**, 2–9 (2009)

24. T.S. Zhang, J. Ma, L.B. Kong, P. Hing, Y.J. Leng, S.H. Chan, J.A. Kilner, Sinterability and ionic conductivity of coprecipitated Ce0.8Gd0.2O2 − δ powders treated via a high-energy ball-milling process. J. Power Sources **124**, 26–33 (2003)

25. H.J. Park, G.M. Choi, The electrical conductivity and oxygen permeation of ceria with alumina addition at high temperature. Solid State Ion. **178**, 1746–1755 (2008)

26. D. Xu, X. Liu, S. Xu, D. Yan, L. Pei, C. Zhu, D. Wang, W. Su, Fabrication and performance of Ce0.85Sm0.15O1.925–Fe₂O₃ electrolytes in IT-SOFCs. Solid State Ion. **192**, 510–514 (2011)

27. T.S. Zhang, J. Ma, S.H. Chan, J.A. Kilner, Grain boundary conduction of Ce0.9Gd0.1O2 − δ ceramics derived from oxalate coprecipitation: effects of Fe loading and sintering temperature. Solid State Ion. **176**, 377–384 (2005)

28. Y.-C. Wu, Y.-Y. Liao, Effect of Ca2+ and Sr2+ doping on the microstructure and cell performance of samaria-doped ceria electrolytes used in solid oxide fuel cells. Int. J. Hydrog. Energy **41**, 13591–13602 (2016)

29. K.C. Anjaneya, J. Manjanna, G.P. Nayaka, V.M. Ashwin Kumar, G. Govindaraj, K.N. Ganesha, Citrate-complexation synthesized Ce0.85Gd0.15O2 − δ (GDC15) as solid electrolyte for intermediate temperature SOFC. Phys. B **447**, 51–55 (2014)

30. G. Chen, H. Kishimoto, K. Yamaji, K. Kuramoto, M. Gong, X. Liu, G. Hackett, K. Gerdes, T. Horita, Chemical reaction

mechanisms between Y_2O_3 stabilized ZrO_2 and Gd doped CeO_2 with PH_3 in coal syngas. J. Power Sources **268**, 904–910 (2014)

31. C.G.M. Lima, T.H. Santos, J.P.F. Grilo, R.P.S. Dutra, R.M. Nascimento, S. Rajesh, F.C. Fonseca, D.A. Macedo, Synthesis and properties of CuO-doped $Ce0.9Gd0.1O2 - \delta$ electrolytes for SOFCs. Ceram. Int. **41**, 4161–4168 (2015)

32. J. Cheng, W. Bao, C. Han, W. Cao, A novel electrolyte for intermediate solid oxide fuel cells. J. Power Sources **195**, 1849–1853 (2010)

33. B. Matović, M. Stojmenović, J. Pantić, A. Varela, M. Žunić, N. Jiraborvornpongsa, T. Yano, Electrical and microstructural properties of Yb-doped CeO_2. J. Asian Ceram. Soc. **2**, 117–122 (2014)

34. L. Guan, S. Le, S. He, X. Zhu, T. Liu, K. Sun, Densification behavior and space charge blocking effect of Bi_2O_3 and Gd_2O_3 Co-doped CeO_2 as electrolyte for solid oxide fuel cells. Electrochim. Acta **161**, 129–136 (2015)

35. Y.-C. Wu, Y.-Y. Liao, Effect of Ca2 + and Sr2 + doping on the microstructure and cell performance of samaria-doped ceria electrolytes used in solid oxide fuel cells. Int. J. Hydrog. Energy **41**, 13591–13602 (2016)

36. N.K. Singh, P. Singh, M.K. Singh, D. Kumar, O. Parkash, Auto-combustion synthesis and properties of $Ce0.85Gd0.15O1.925$ for intermediate temperature solid oxide fuel cells electrolyte. Solid State Ion. **192**, 431–434 (2011)

37. S. Kumar, S. Gautam, T.K. Song, K.H. Chae, K.W. Jang, S.S. Kim, Electronic structure study of Co doped CeO_2 nanoparticles using X-ray absorption fine structure spectroscopy. J. Alloys Compd. **611**, 329–334 (2014)

38. K. Huang, J.B. Goodenough, *Performance Characterization Techniques for a Solid Oxide Fuel Cell (SOFC) and its Components[M]* (Elsevier, Amsterdam, 2009)

39. E. Drożdż, J. Wyrwa, K. Schneider, M. Rękas, Electrical properties of silica-doped 3 mol% yttria-stabilized tetragonal zirconia. J. Mater. Sci. **52**, 674–685 (2016)

40. R.K. Lenka, T. Mahata, A.K. Tyagi, P.K. Sinha, Influence of grain size on the bulk and grain boundary ion conduction behavior in gadolinia-doped ceria. Solid State Ion. **181**, 262–267 (2010)

41. D. Zhou, Y. Xia, J. Zhu, W. Guo, J. Meng, Preparation and electrical properties of new oxide ion conductors $Ce6 - xGdxMoO15 - \delta$ ($0.0 \leq x \leq 1.8$). J. Am. Ceram. Soc. **92**, 1042–1046 (2009)

42. B. Ji, C. Tian, C. Wang, T. Wu, J. Xie, M. Li, Preparation and characterization of $Ce0.8Y0.2 - xCuxO2 - \delta$ as electrolyte for intermediate temperature solid oxide fuel cells. J. Power Sources **278**, 420–429 (2015)

43. Y. Zheng, M. Zhou, L. Ge, S. Li, H. Chen, L. Guo, Effect of Fe2O3 on Sm-doped ceria system solid electrolyte for IT-SOFCs. J. Alloys Compd. **509**, 546–550 (2011)

44. T.S. Zhang, J. Ma, Y.J. Leng, S.H. Chan, P. Hing, J.A. Kilner, Effect of transition metal oxides on densification and electrical properties of Si-containing $Ce0.8Gd0.2O2 - \delta$ ceramics. Solid State Ion. **168**, 187–195 (2004)

45. W. Sun, Z. Shi, J. Qian, Z. Wang, W. Liu, In-situ formed $Ce0.8Sm0.2O2 - \delta @Ba(Ce, Zr)1 - x(Sm, Y)xO3 - \delta$ core/shell electron-blocking layer towards $Ce0.8Sm0.2O2 - \delta$-based solid oxide fuel cells with high open circuit voltages. Nano Energy **8**, 305–311 (2014)

46. M. Yashima, Invited review: some recent developments in the atomic-scale characterization of structural and transport properties of ceria-based catalysts and ionic conductors. Catal. Today **253**, 3–19 (2015)

47. L. Zhang, F. Liu, K. Brinkman, K.L. Reifsnider, A.V. Virkar, A study of gadolinia-doped ceria electrolyte by electrochemical impedance spectroscopy. J. Power Sources **247**, 947–960 (2014)

48. A. Sawka, A. Kwatera, Deposition of Sm_2O_3-doped CeO_2 layers using the MOCVD method. Ceram. Int. **42**, 1446–1452 (2016)